Available online at www.sciencedirect.com
ScienceDirect
Polymer 47 (2006) 6446–6456
polymer
www.elsevier.com/locate/polymer

Distribution analyses of multi-modal dynamic light scattering data

Mitsuhiro Shibayama [a,b,*], Takeshi Karino [b], Satoshi Okabe [a]

[a] Neutron Science Laboratory, The Institute for Solid State Physics, The University of Tokyo, Tokai, Naka-gun, Ibaraki 319-1106, Japan
[b] CREST, Japan Science and Technology Agency, 4-1-8 Honcho, Kawaguchi, Saitama 332-0012, Japan

Received 14 April 2006; received in revised form 21 June 2006; accepted 25 June 2006
Available online 24 July 2006

Abstract

A method of data analysis for dynamic light scattering is proposed to evaluate the weight fraction, $w(R_h)$, of a small amount of large aggregates in a dilute solution, where R_h is the hydrodynamic radius. We examined the time-correlation function of scattering intensity for model multi-modal systems, i.e., mixtures of latex solutions having different particle sizes and of polystyrene standard solutions having different molecular weights, by properly taking into account the unknown fractions, $w(R_h)$, and scattering intensities of individual components. We derived an equation to evaluate the weight fractions of the components. The validity of this method was verified by successfully reconstructing the observed correlation functions having fast and slow modes. As a demonstration, the fraction of aggregates in a thermosensitive polymer solution in water was evaluated as a function of temperature.

Keywords: Dynamic light scattering; Aggregates; CONTIN

1. Introduction

Dynamic light scattering (DLS) has been widely used in physical chemistry, colloid chemistry, polymer science, biochemistry and biophysics, medical science, etc., as well as product development and quality inspection in industry. It allows evaluation of the size and size distribution of colloidal particles in a dispersant [1] and polymer chains in a solution [2,3]. Not only for size evaluation but also for slow dynamics, gelation processes, and vitrification processes have been investigated by DLS [4–6]. Owing to advances in laser light scattering, such as avalanche photo diode detectors and computers, the performance of modern DLS instruments covers 10 ns to 10 s [7]. It is well known that light scattering is very sensitive to large objects in a specimen. That is why optical purification is of great significance. It means, on the other hand, DLS can be used to characterize association state of polymers or colloid particles. Evaluation of agglutinated particles is a typical example of applications of DLS in immunoassay [8].

The observable quantity in DLS is the time-correlation function of the scattering intensity, i.e., the so-called second-order correlation function, $g^{(2)}(\tau)$. The decay rate distribution function $G(\Gamma)$ obtained by inverse Laplace transform of $g^{(2)}(\tau)$, in principle, has information about the distribution of the dispersed particles and/or solutes, e.g., the weight fraction of the particles, $w(R_h)$, where τ, Γ, and R_h are the decay time, the characteristic decay rate, and the hydrodynamic radius of the dispersed objects or solutes, respectively. However, $w(R_h)$ cannot be simply obtained from $G(\Gamma)$ because $g^{(2)}(\tau)$ is a complicated function of $w(R_h)$ and the structure factor $S(q)$. Provencher and Stepanek proposed a simultaneous fit of several autocorrelation functions measured at different scattering angles [9]. They applied this method to semi-dilute polymer solutions and plasticized polymers, in addition to microemulsion networks. Vega and coworkers proposed two methods to obtain latex particle size distribution by DLS [10,11]. Antony et al. reported the feasibility of DLS to detect agglutination of antigen-carrier particles mediated by antibody [12]. However, these treatments lack in the consideration of

* Corresponding author. Neutron Science Laboratory, The Institute for Solid State Physics, The University of Tokyo, Tokai, Naka-gun, Ibaraki 319-1106, Japan. Tel.: +81 29 287 8904; fax: +81 29 283 3922.
E-mail address: sibayama@issp.u-tokyo.ac.jp (M. Shibayama).

0032-3861/$ - see front matter © 2006 Elsevier Ltd. All rights reserved.
doi:10.1016/j.polymer.2006.06.060

the q-dependence of the solutes, i.e., the intensity contribution to the time-correlation function via $S(q)$. Hence, it was unable to extract information about $w(R_h)$. Kanao et al. investigated aggregate-containing poly(n-hexyl isocyanate) solutions by static and dynamic light scattering and discussed the conformation of the aggregates [13]. However, they did not explicitly show the relationship between $G(\Gamma)$ and $w(R_h)$ and their analysis was limited to discussion of the conformation of aggregates. To our knowledge, there have been only a few papers that properly deal with this problem. Wu et al. characterized polymer mixtures made of individual linear chains and clusters. They considered the contribution of $S(q)$ and obtained the ratio of clusters to molecularly-dispersed polymer chains by using a set of polystyrene mixtures with large- and small-molecular weights. In addition, they applied this method to characterize the cluster size of PES-C (phenolphthalein poly(ether sulfone)) [14] and other thermoplastic polymers [15,16].

As was addressed by Wu et al. [14,17], characterization of aggregated systems having a bimodal or multi-modal distribution is important because of their industrial and pharmaceutical applications. In this paper, we propose a method to evaluate the fraction of associated clusters in colloidal dispersions as well as in polymer solutions. We carefully examined the time-correlation function for model multi-modal systems, i.e., mixtures of latex solutions having different particle sizes and of polystyrene standard solutions having different molecular weights. We properly took into account the contributions of the fractions, $w(R_h)$, and scattering intensities of individual components of the time–intensity correlation function, $g^{(1)}(\tau)$, and derived an equation to evaluate the weight fractions of the components. This, in turn, was used to reconstruct the observed correlation functions. Furthermore, we applied this method to evaluate the weight fraction of aggregates in an aqueous solution of a thermosensitive polymer carrying hydrophobic side group [18].

2. Theoretical background

2.1. Time-correlation functions and the decay rate distribution function

The observable quantity of DLS is the time-correlation function of the scattering intensity, i.e., the so-called second-order correlation function, $g^{(2)}(\tau)$, which is converted to the first-order correlation function, $g^{(1)}(\tau)$, via Siegert relation [19],

$$g^{(1)}(\tau) = \sqrt{g^{(2)}(\tau) - 1} \tag{1}$$

where τ is the decay time. $g^{(1)}(\tau)$ is given by

$$g^{(1)}(\tau) = \exp\left[-Dq^2\tau\right] \tag{2}$$

for Brownian objects moving with the translational diffusion coefficient, D. Here, q is the magnitude of the scattering vector defined by $q = |\mathbf{q}| = (4\pi n/\lambda)\sin(\theta/2)$, where n is the refractive index of the scattering medium, λ is the wavelength of the light in vacuum, and θ is the scattering angle. Hence, the diffusion coefficient is obtained by

$$D = -\frac{1}{2q^2}\lim_{\tau\to 0}\frac{\mathrm{d}}{\mathrm{d}\tau}\ln\left[g^{(2)}(\tau) - 1\right] \tag{3}$$

The size of the diffusing object, i.e., the hydrodynamic radius, R_h, is obtained via Stokes–Einstein equation:

$$R_h = \frac{kT}{6\pi\eta D} \tag{4}$$

where η is the viscosity of the solvent, k is the Boltzmann constant, and T is the absolute temperature. This argument, however, cannot be simply applied to systems consisting of multi-modal objects, such as mixtures of latexes having different sizes or polymer solutions with multi-modal molecular weight distributions. In order to obtain the particle distribution, inverse Laplace transform of $g^{(1)}(\tau)$ has been commonly employed because $g^{(1)}(\tau)$ is obtained by Laplace transform of the distribution function, $G(\Gamma)$,

$$g^{(1)}(\tau) = \int_0^\infty G(\Gamma)\mathrm{e}^{-\Gamma\tau}\,\mathrm{d}\Gamma \tag{5}$$

$G(\Gamma)$ is obtained by inverse Laplace transform of $g^{(1)}(\tau)$. Various algorithms including CONTIN [20] have been widely used [2]. However, as is discussed in the following subsection, the relationship between $g^{(1)}(\tau)$ and $G(\Gamma)$ is not trivial.

2.2. The correlation function

The first-order time-correlation function, i.e., the correlation function for the scattering amplitude, $C^{(1)}(\tau,q)$ is given by

$$C^{(1)}(\tau,q) = \left\langle \sum_{i,j}^{N} E(\mathbf{r}_i,t)E^*(\mathbf{r}_j,t+\tau)\exp\left[\mathrm{i}\mathbf{q}\cdot\left\{\mathbf{r}_i(t) - \mathbf{r}_j(t+\tau)\right\}\right]\right\rangle \tag{6}$$

where $E(\mathbf{r}_i,t)$ is the scattering field at position $\mathbf{r}_i$ and time t. In the case of an ensemble of non-interacting particles, the time-dependent phase average in Eq. (6) can be divided into space- and time-averages by mode-decoupling of time and space averages,

$$\begin{aligned}&\left\langle \exp\left[\mathrm{i}\mathbf{q}\cdot\left\{\mathbf{r}_i(t) - \mathbf{r}_j(t+\tau)\right\}\right]\right\rangle \\ &\quad\cong \left\langle \exp\left[\mathrm{i}\mathbf{q}\cdot\left\{\mathbf{r}_i(t) - \mathbf{r}_j(t)\right\}\right]\right\rangle\left\langle \exp\left[\mathrm{i}\mathbf{q}\cdot\left\{\mathbf{r}_j(t) - \mathbf{r}_j(t+\tau)\right\}\right]\right\rangle \\ &\quad= \left\langle \exp\left[\mathrm{i}\mathbf{q}\cdot\mathbf{r}_{ij}(t)\right]\right\rangle\left\langle \exp[\mathrm{i}\mathbf{q}\cdot\delta\mathbf{r}(\tau)]\right\rangle\end{aligned} \tag{7}$$

Here, $\mathbf{r}_{ij}(t) \equiv \mathbf{r}_i(t) - \mathbf{r}_j(t)$ and $\delta\mathbf{r}(\tau) \equiv \mathbf{r}(t) - \mathbf{r}(t+\tau)$. Hence, the time-correlation function is obtained by

$$C^{(1)}(\tau,q) \cong \sum_{i,j}^{N}\left\langle E(\mathbf{r}_i)E^*\left(\mathbf{r}_j\right)\exp\left[\mathrm{i}\mathbf{q}\cdot\mathbf{r}_{ij}(t)\right]\right\rangle\left\langle \exp[\mathrm{i}\mathbf{q}\cdot\delta\mathbf{r}(\tau)]\right\rangle \tag{8}$$

Note that the assumption made in Eq. (7) is also applicable to polymer solutions because the q-range employed is much smaller than the radius of gyration of polymer chains in

most cases and only translational diffusion of polymer chains is taken into account. In Eq. (8), the first average gives the scattering intensity of the particle. The scattering intensity is obtained with the form factor $P(qR)$,

$$C^{(1)}(\tau=0,q)=NV^2P(qR) \tag{9}$$

where R and V are the radius and the volume of the particle, respectively, and N is the number of particles in the irradiated volume. In the case of spheres, $P(qR)=\Phi^2(qR)$, and $\Phi(qR)$ is given by

$$\Phi(qR)=3\frac{\sin(qR)-qR\cos(qR)}{(qR)^3} \tag{10}$$

On the other hand, the second average in Eq. (8) is related to the Brownian motion of the scattering object, and the Brownian motion is characterized as:

$$W(\delta\mathbf{r},t)=\frac{1}{(4\pi Dt)^{3/2}}\exp\left[-\frac{\delta\mathbf{r}^2}{4Dt}\right] \tag{11}$$

Eq. (11) readily leads to,

$$\langle\exp[i\mathbf{q}\cdot\delta\mathbf{r}(t)]\rangle=\int\exp[i\mathbf{q}\cdot\delta\mathbf{r}(t)]W(\delta\mathbf{r},t)d\delta\mathbf{r}=\exp\left[-Dq^2t\right] \tag{12}$$

therefore, $C^{(1)}(\tau,q)$ for spherical objects is given by

$$C^{(1)}(\tau,q)\equiv\langle E(t,q)E^*(t+\tau,q)\rangle=NV^2\Phi^2(qR)\exp\left[-Dq^2\tau\right] \tag{13}$$

2.3. Bimodal distribution of colloidal particles

Now, let us discuss the correlation function for a bimodal distribution of spherical objects having the radii R_1 and R_2 ($R_1<R_2$). The correlation function is now given by

$$C^{(1)}(\tau,q)=\left\langle A_1(q)\exp\left[-D_1q^2\tau\right]+A_2(q)\exp\left[-D_2q^2\tau\right]\right\rangle \tag{14}$$

where

$$A_i(q)\equiv N_iV_i^2\Phi^2(qR_i) \tag{15}$$

The normalized-first-order correlation function is thus given by

$$g^{(1)}(\tau,q)\equiv\frac{C^{(1)}(\tau,q)}{A_1(q)+A_2(q)}=\frac{1}{A_1(q)+A_2(q)}\times\left\langle A_1(q)\exp\left[-D_1q^2\tau\right]+A_2(q)\exp\left[-D_2q^2\tau\right]\right\rangle \tag{16}$$

Note that $g^{(1)}(\tau,q)$ is reduced to unity by approaching $\tau=0$, i.e.,

$$g^{(1)}(\tau\to0,q)=\frac{1}{A_1(q)+A_2(q)}\langle A_1(q)+A_2(q)\rangle\to1$$

$$g^{(1)}(\tau\to\infty,q)\to0$$

The number of spheres is related to the mass (weight) fractions ($i=1$ or 2) by

$$w_i=\frac{N_iM_i}{\sum_i N_iM_i} \tag{17}$$

On the other hand, the mass concentration c_i of the particles of kind i is given by

$$c_i=\frac{N_iM_i}{V_{\text{total}}}\left[\text{g/cm}^3\right],\ \ c=\sum_i c_i \tag{18}$$

Here, V_{total} and M_i are the total volume of the solution and the mass (or molecular weight) of the particles of kind i. For example, in the case of polystyrene (PS) latex, M_i is simply given by

$$M_i=\rho\frac{4\pi}{3}R_i^3 \tag{19}$$

where ρ is the mass density and R_i is the radius of the particle i.

Let us represent Eq. (15) in terms of w_i instead of N_i. N_i is simply given by

$$\begin{pmatrix}N_1\\N_2\end{pmatrix}=\frac{1}{W}\begin{pmatrix}w_1/M_1\\w_2/M_2\end{pmatrix} \tag{20}$$

Here, $W\equiv\sum_i N_iM_i$ is the total mass of the solute in V_{total}. By using Eqs. (19) and (20), one can rewrite Eq. (15) as follows,

$$A_i(q)=N_iV_i^2\Phi^2(qR_i)\sim w_iR_i^3\Phi^2(qR_i) \tag{21}$$

Hence, the peak height (or area) is proportional to w_i, R_i^3, and $\Phi^2(qR_i)$.

2.4. Distribution function

Now let us relate $g^{(1)}(\tau,q)$ to $A_i(q)$. Eq. (16) simply leads to

$$\begin{aligned}g^{(1)}(\tau,q)&=\frac{1}{A_1(q)+A_2(q)}\left\langle A_1(q)\exp\left[-D_1q^2\tau\right]+A_2(q)\exp\left[-D_2q^2\tau\right]\right\rangle\\&=\frac{A_1(q)}{A_1(q)+A_2(q)}\exp\left[-D_1q^2\tau\right]+\frac{A_2(q)}{A_1(q)+A_2(q)}\exp\left[-\mathrm{D}_2q^2\tau\right]\end{aligned} \tag{22}$$

If each mode is very sharp, a comparison of Eqs. (5) and (22) leads to

$$G(\Gamma)=\frac{A_1(q)}{A_1(q)+A_2(q)}\delta\left(\Gamma-D_1q^2\right)+\frac{A_2(q)}{A_1(q)+A_2(q)}\delta\left(\Gamma-D_2q^2\right) \tag{23}$$

Here, $\delta(x)$ is the Dirac delta function. Hence, in general, the distribution function for n-modal correlation function is given by

$$G(\Gamma) = \sum_i^n \frac{A_i(q)}{\sum_j A_j(q)} \delta\left(\Gamma - D_i q^2\right) \tag{24}$$

Here, $\sum_j A_j(q)$ is the total area of $G(\Gamma)$. Let us rewrite Eq. (24) in a more explicit form, for example, for a binary system,

$$G(\Gamma) = \frac{w_1 R_1^3 \Phi^2(qR_1)}{w_1 R_1^3 \Phi^2(qR_1) + w_2 R_2^3 \Phi^2(qR_2)} \delta\left(\Gamma - D_1 q^2\right) + \frac{w_2 R_2^3 \Phi^2(qR_2)}{w_1 R_1^3 \Phi^2(qR_1) + w_2 R_2^3 \Phi^2(qR_2)} \times \delta\left(\Gamma - D_2 q^2\right) \text{ (binary system)} \tag{25}$$

The hydrodynamic radius of the particles of kind i is obtained by the Stokes–Einstein law,

$$R_{h,i} = \frac{kT}{6\pi\eta D_i} = \frac{kT}{6\pi\eta} \frac{q^2}{\Gamma_i} \tag{26}$$

The peak height (or area) $G(\Gamma_i)$ is given by

$$G(\Gamma_i) = \frac{w_i R_i^3 \Phi^2(qR_i)}{\sum_j A_j(q)} \tag{27}$$

From Eq. (27), the weight fraction w_i is readily obtained by

$$w_i = \frac{G(\Gamma_i) \sum_i A_i(q)}{R_i^3 \Phi^2(qR_i)} \propto \frac{G(\Gamma_i)}{R_i^3 \Phi^2(qR_i)} \tag{28}$$

3. Experimental section

3.1. Samples

Two types of polystyrene (PS) latex were purchased from Duke Science Corp., U.S.A. The PS latex solutions were coded as L0 (PSS; the diameter $2R_1 = 50 \pm 2.0$ nm) and L100 (PSL; $2R_2 = 596 \pm 6$ nm). The values of standard deviation of the radius were 6.7 and 7.7 nm, respectively. The concentration of PS in water was ca. 1 wt%. The latex solutions were diluted by 1000 times and then five samples were prepared by mixing the two with different compositions, namely, 100/0 (L0), 75/25 (L25), 50/50 (L50), 25/75 (L75), and 0/100 (L100). Here, the sample codes are given in the parentheses. Standard polystyrene samples were also purchased from Polymer Source, Inc., Montreal, Canada. The molecular weights of the PS samples were $M_n = 11.0 \times 10^3$ and $M_w = 11.5 \times 10^3$ for P0 and $M_n = 102.6 \times 10^3$ and $M_w = 108.7 \times 10^3$ for P100, where M_n and M_w are the number- and weight-average molecular weight, respectively. The sample specification is given in Table 1. These PS samples were dissolved in cyclohexane. The polymer concentrations were 1.0 wt%, both for P0 and P100. Five PS solutions were prepared by mixing these two stock solutions with different compositions, namely, 100/0 (P0), 75/25 (P25), 50/50 (P50), 25/75 (P75), and 0/100 (P100).

Table 1
Polystyrene samples

Sample code	M_n	M_w	M_w/M_n
P0	1.10×10^4	1.15×10^4	1.05
P100	10.26×10^4	10.87×10^4	1.06

3.2. DLS

Dynamic Light Scattering (DLS) measurements were carried out on a DLS/SLS-5000 compact goniometer, ALV, Langen, Germany, coupled with an ALV photon correlator. A 22-mW helium–neon laser (Uniphase Co. Ltd., U.S.A.) was used as the light source. Although the laser power was relatively weak, the output photon count rate was enhanced by about 50 times when compared to the conventional pinhole system used in our laboratory. This was made by employing a set of static and dynamic enhancers (devices to enhance the photon counting rate) and a high quantum efficient avalanche photo diode detection system. The characteristic decay time distribution function, $G(\Gamma^{-1})$, was obtained from $g^{(2)}(\tau)$ with an inverse Laplace transform program (a constrained regularization program, CONTIN provided by ALV). The temperature was regulated to 20.0 ± 0.1 °C for PS latex and to 34.5 ± 0.1 °C for standard PS solutions in cyclohexane. The scattering angle range was 45–150°.

4. Results and discussion

4.1. Model system – bimodal distribution of PS latex

Fig. 1 shows (a) the second-order time-correlation functions, $g^{(2)}(\tau)$ and (b) their semi-logarithmic plots, $\ln [g^{(2)}(\tau) - 1]$ vs τ, for the individual latex solutions, i.e., L0 (PSS) and L100 (PSL) obtained at the scattering angle $\theta = 90°$. As shown in the figure, each of $g^{(2)}(\tau,q)$s is a single-decay function, and the corresponding distribution function clearly shows a unimodal distribution. The translational diffusion coefficient, D, of the latex particles can be obtained from the first cumulant of $[g^{(2)}(\tau) - 1]$ with Eq. (3). The hydrodynamic radius, R_h, of the particles is evaluated by the slope in Fig. 1b (the solid line) with Eq. (4). The cumulant analysis gave $R_h = 29.1$ and 315 nm, respectively, for L0 and L100.

Fig. 2 shows the distribution function, $G(\Gamma^{-1})$, obtained by CONTIN analysis of $g^{(2)}(\tau)$s in Fig. 1 as a function of the characteristic time Γ^{-1} and not the characteristic decay rate Γ. As expected, each of $G(\Gamma^{-1})$ shows a single peak. From the peak position, the hydrodynamic radius was obtained by

$$R_h = \frac{kT}{6\pi\eta} q^2 \Gamma_{peak}^{-1} \tag{29}$$

where Γ_{peak}^{-1} is the characteristic decay time at the peak. The evaluated values were $R_h = 29.1$ and 322 nm, respectively, for L0 and L100. Table 2 shows comparison of the evaluated hydrodynamic radii for L0 and L100 by the two methods. Though these

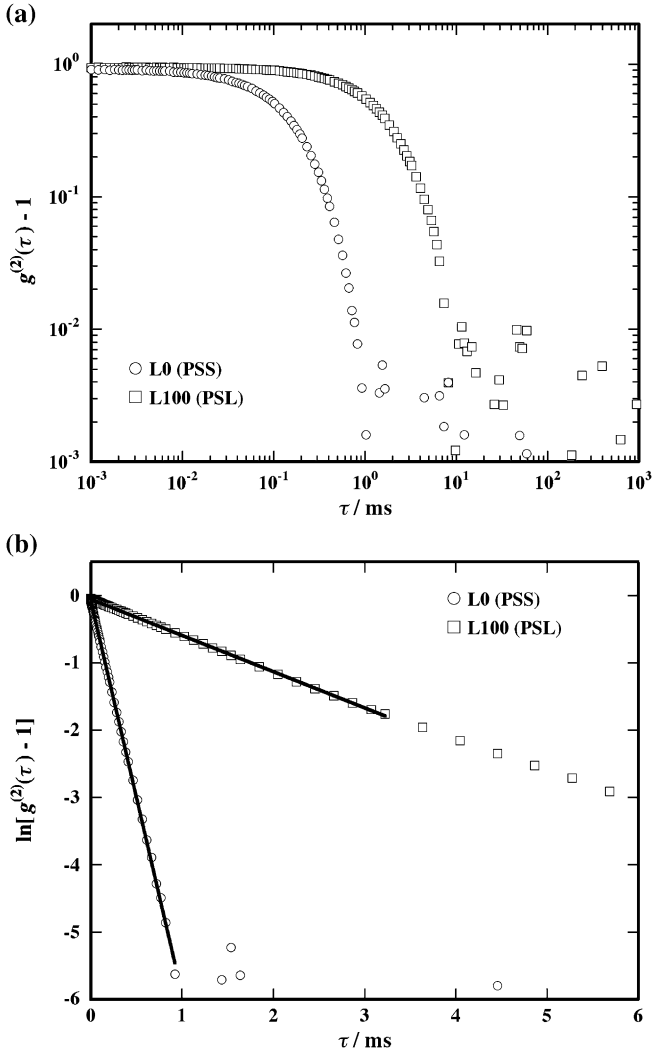

Fig. 1. (a) The second-order time-correlation functions of latex solutions L0 (PSS) and L100 (PSL) observed at $\theta = 90°$. (b) The cumulant analysis of L0 (PSS) and L100 (PSL).

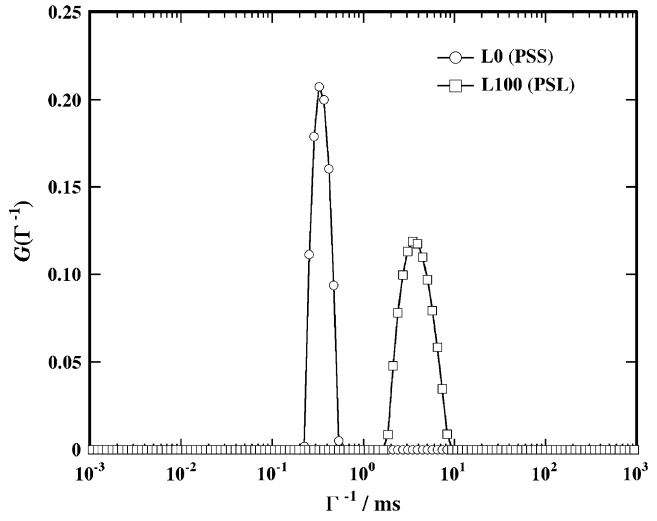

Fig. 2. Distribution functions of latex solutions L0 (PSS) and L100 (PSL).

Table 2
Comparison of R_h values obtained by cumulant and CONTIN methods

	Nominal	Cumulant	CONTIN
L0 (nm)	25.0	29.1	29.1
L100 (nm)	298	315	322

values are somewhat larger than the catalogue values, both agree well to each other within the experimental error.

Fig. 3 shows (a) $g^{(2)}(\tau)$ and (b) $G(\Gamma^{-1})$ for a 50/50 (w/w) mixture of PSS and PSL, i.e., L50, obtained at $\theta = 90°$. It is difficult to resolve the PSS component in $g^{(2)}(\tau)$, while a small peak is observed in $G(\Gamma^{-1})$. This figure clearly shows that $G(\Gamma^{-1})$ does not directly show the fractions of the fast (small) and slow (large) components, but is heavily weighted to the large component.

Fig. 4 shows the composition dependence of $G(\Gamma^{-1})$s for the pure solutions (L0 and L100) and mixtures (L25, L50, and L75). The sharp peak of PSS (the fast component) drastically decreases with increasing PSL fractions, while that of

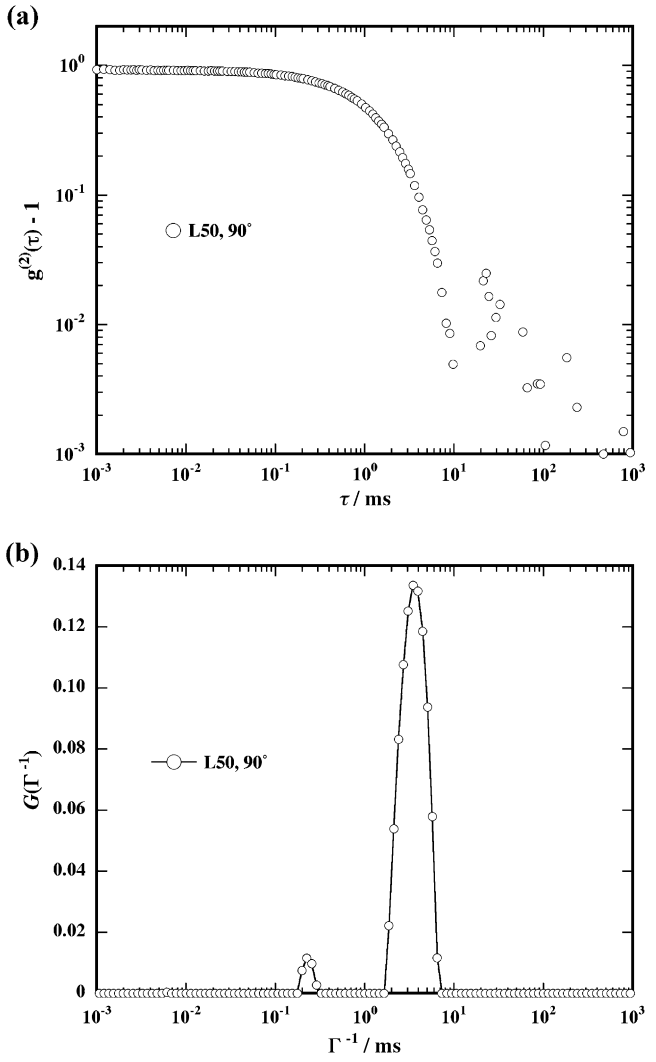

Fig. 3. (a) Time–intensity correlation function and (b) the distribution function of latex solutions having bimodal distribution (L50).

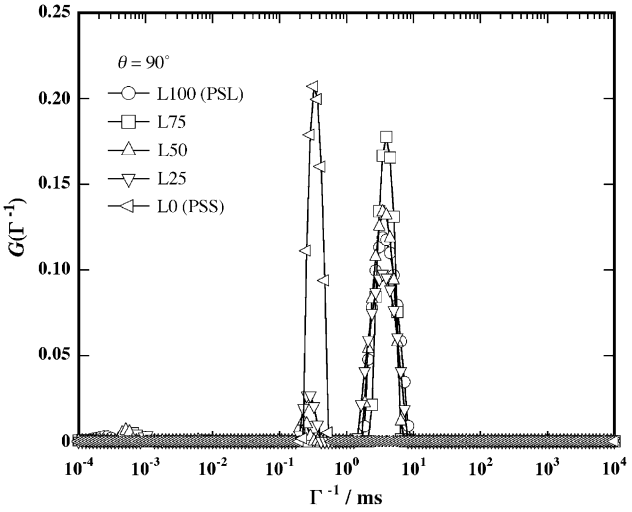

Fig. 4. Distribution function of bimodal latex solutions having various weight fractions. The scattering angle is 90°.

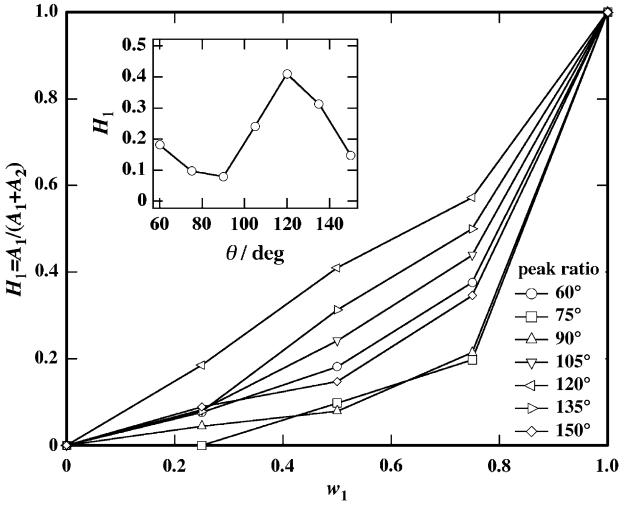

Fig. 6. The peak height fraction of PSS, H_1, as functions of the weight fraction, w_1. The inset shows the scattering angle, θ, dependence of the peak height fraction of L0, H_1, for the case of $w_1 = 0.5$.

PSL (the slow component) decreases rather gradually with decreasing PSL component. It should be noted that the peak positions are roughly independent of the composition. Fig. 5 shows the scattering angle dependence of $G(\Gamma^{-1})$s for L50. By increasing θ, the peaks (indicated by the arrows) shift toward the direction of faster decay time by keeping bimodality. Note that the relative heights of the peaks change non-systematically with increasing θ.

Fig. 6 shows the relative peak height of the fast mode, $H_1 = A_1/(A_1 + A_2)$, as a function of the weight fraction of the fast-mode component (PSS), w_1. As shown in the figure, the value is strongly biased by the slow- (large-)component, i.e., PSL, with a different weight depending on θ. In addition, it does not seem to have a simple relationship between H_1 and w_1. As a matter of fact, the θ dependence of H_1, for the case of $w_1 = 0.5$ plotted in the inset of Fig. 6, clearly shows an oscillation of H_1 with θ.

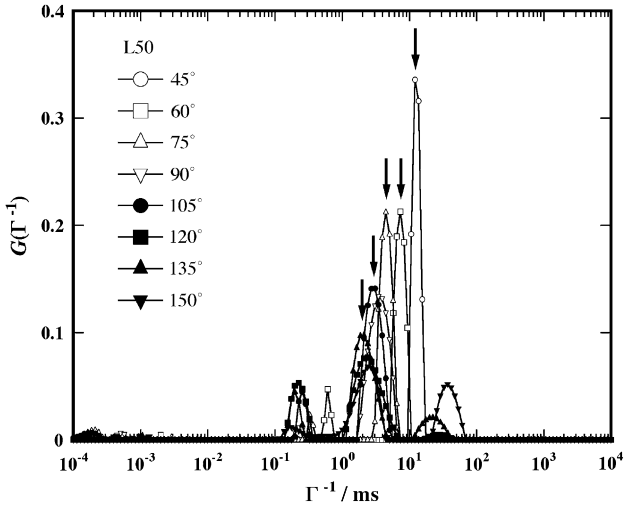

Fig. 5. Distribution functions of bimodal latex solutions. Scattering angle dependence.

4.2. Reconstruction of $g^{(2)}(\tau)$ and $G(\Gamma^{-1})$

According to the discussion in Section 2, it is clear that the shape of $G(\Gamma^{-1})$ is strongly affected by the scattering intensities of the individual scatterers. Fig. 7 shows the normalized static scattering intensity functions, $P(qR)$, for PSL (L100) and PSS (L0), where $P(qR)$ is defined by

$$P(qR) \equiv \frac{C^{(1)}(\tau = 0, q)}{NV^2} = \Phi^2(qR) \tag{30}$$

The open circles denote the observed functions and the dashed and solid curves indicate the calculated scattering functions with a size distribution of $\Delta R/R = 0$ and 0.08, respectively. In the case of PSL, a value $R = 341$ nm was

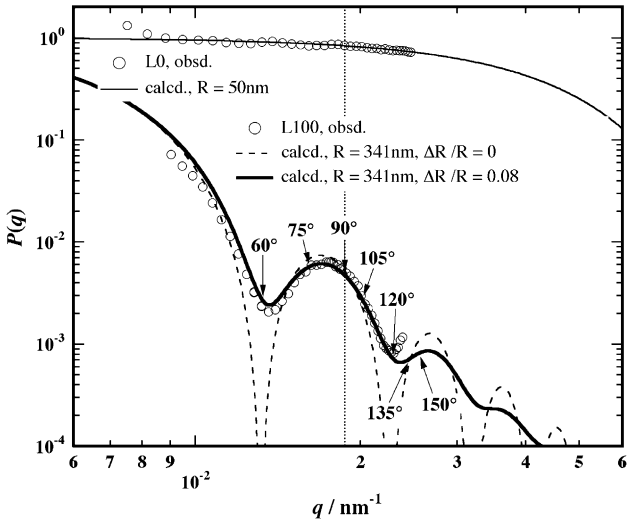

Fig. 7. Static light scattering intensity functions for L0 and L100. Symbols: obsd., lines: fitted functions $P(qR)$s. The vertical dotted line indicates the value of q corresponding to the scattering angle of 90°.

obtained by curve fitting. Although this value is somewhat larger than the catalogue value $(596 \pm 6)/2$ nm and those obtained by DLS ($R = R_h = 316$ nm by cumulant and 322 nm by CONTIN analysis; Table 2), these values can be regarded to be within experimental error. On the other hand, the observed intensity curve for PSS is a monotonously decreasing function of q with no scattering maxima. The best fit with Eq. (9) gave $R = 50$ nm, which was somewhat larger than the nominal value $R = R_1 = 25$ nm. The bottom line, however, lies in that $P(qR)$ is strongly dependent on the size of the scatterers and affects the analysis of the $G(\Gamma^{-1})$. For example, in the case of a DLS measurement of L50 at $\theta = 90°$ (the position of the vertical dotted line), the weighting factor originated from $P(qR)$s for a mixture of PSS and PSL could be about 100 times. The numbers in the figure anchored to $P(qR)$ are the scattering angles. This curve with these values clearly indicates that the weighting factor, $P(qR)$, is strongly q-dependent. This is the reason why the plot of the inset of Fig. 6 has an oscillation. As a matter of fact, the variation of H_1 with θ is qualitatively inverse of the variation of $P(qR)$ with θ.

Eq. (25) and the above discussion indicate that $G(\Gamma^{-1})$ is uniquely determined with the form factors, $P(qR)$, the radius of the spheres, R_i, and the concentrations if the system consists of spherical particles having a sharp bimodal distribution. Fig. 8 shows the reconstructed (a) $g^{(2)}(\tau)$ and (b) $G(\Gamma^{-1})$. Note that the experimentally-observed values for R_1 and R_2 were used for reconstruction. Therefore, this reconstruction procedure can stand-alone. Though the peak width of the slow component cannot be well reproduced, the shape of $g^{(2)}(\tau)$ and the peak positions are well recovered. This statement is correct whenever the particle factors of the component are known, in another word, the particle sizes and their distributions are known.

It is important to generalize this method to any given system. In reality, each set of particles subjected to characterization usually has a relatively broad size-distribution. This leads to a significant smearing in the form factor. Hence, it is more realistic to employ an asymptotic scattering function instead of the theoretical particle factor for spheres with a given radius. In such a case, the form factor in Eq. (30) can be replaced by either a constant or a power-law function as shown in Fig. 9. The cross-over $qR = 1.78$ is obtained by extrapolating the asymptotic functions given by

$$P(qR) \approx \overline{\Phi}^2(qR) = \begin{cases} 1 & qR \le 1.78 \\ 1.78^4 (qR)^{-4} & qR > 1.78 \end{cases} \tag{31}$$

Note that this asymptotic function $P(qR) \sim q^{-4}$ for $qR = 1.78$ is nothing but a Porod scattering function for a two-phase system with sharp interface [21,22]. Hence, the weighting function is now given by

$$\overline{A}_i(q) = w_i R_i^3 \overline{\Phi}^2(qR_i) \tag{32}$$

The fraction w_i in Eq. (32) can be evaluated by replacing $A_i(q)$ in Eq. (28) by $\overline{A}_i(q)$. Note that Eq. (32) can be further

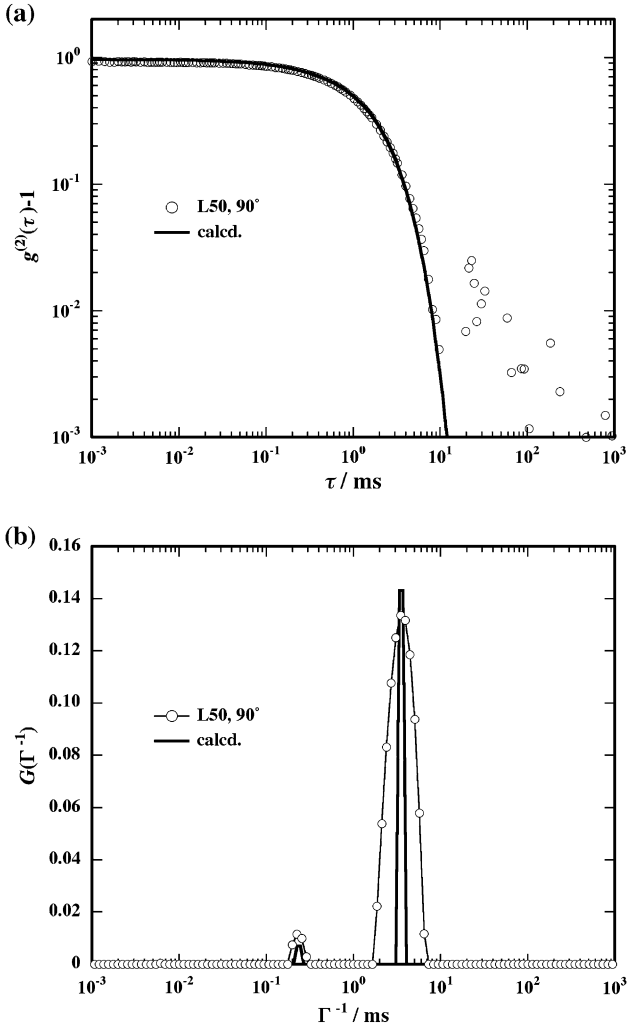

Fig. 8. (a) The reconstructed correlation and (b) distribution functions for the 50/50 mixture of polystyrene latex.

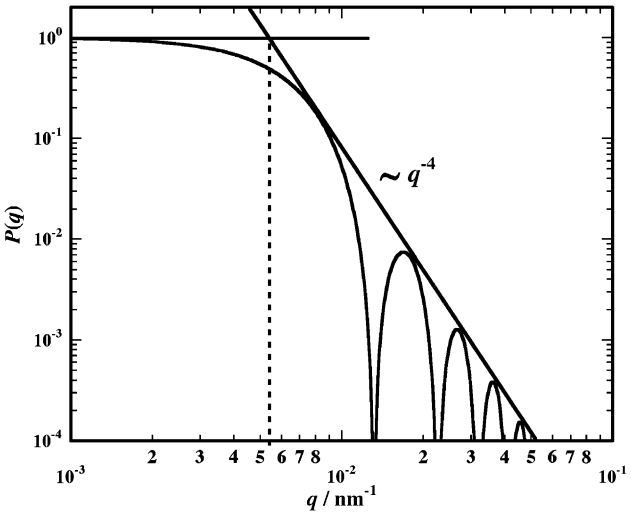

Fig. 9. Comparison of the scattering functions for spheres and the asymptotic behavior of the scattering intensity functions for hard spheres.

simplified for the case of R_1, $R_2 > 1.78/q$. In this case, $P(qR) \propto R^{-4}$, which leads to

$$\overline{A}_i(q) = w_i R_i^3 P(qR_i) \propto w_i/R_i \tag{33}$$

Hence, the peak heights of $G\left(\Gamma_i^{-1}\right)$ are simply proportional to w_i/R_i. On the other hand, if both the radii or either radius R_1 or R_2 is smaller than this criterion, i.e., $qR_i = 1.78$, w_i becomes to have different R_i-dependence and/or q-dependence as given by

$$w_1 = \frac{G(\Gamma_1)/R_1^3\overline{\Phi}^2(qR_1)}{\sum_j G\left(\Gamma_j\right)/R_j^3\overline{\Phi}^2\left(qR_j\right)} = \begin{cases} \dfrac{G(\Gamma_1)/R_1^3}{G(\Gamma_1)/R_1^3 + G(\Gamma_2)/R_2^3} & (qR_1, qR_2 \le 1.78) \\ \dfrac{G(\Gamma_1)/R_1^3\ [\mathrm{nm}^3]}{G(\Gamma_1)/R_1^3\ [\mathrm{nm}^3] + G(\Gamma_2)R_2\ [\mathrm{nm}]\ q^4\ [\mathrm{nm}^{-4}]/1.78^4} & (qR_1 < 1.78 \le qR_2) \\ \dfrac{G(\Gamma_1)R_1}{G(\Gamma_1)R_1 + G(\Gamma_2)R_2} & (1.78 \le qR_1, qR_2) \end{cases} \tag{34}$$

This is the reason why no simple relationship was observed in Fig. 6.

Fig. 10 shows the comparison of the fraction, H_1, of the observed and reconstructed distribution functions for L50 at $\theta = 90°$. Plots (a) and (b) are obtained by using the peak areas and peak heights of $G\left(\Gamma_i^{-1}\right)$s, respectively. Plots (c) and (d) are obtained by using the exact function, $\Phi^2(qR)$, and the asymptotic function, $\overline{\Phi}^2(qR)$, respectively. As shown in the figure, the reconstructed H_1 with the asymptotic function agrees reasonably well to the observed value with the peak height. Note that plot (d) also gives an acceptable agreement with the observed data even when an asymptotic scattering function is employed for the evaluation of the scattering intensity contribution to the time-correlation function. Therefore, it is concluded that the weight fractions of the particles in a solution can be, at least semi-quantitatively, evaluated from the decay rate (or time) distribution function, $G(\Gamma_i)$ (or $G\left(\Gamma_i^{-1}\right)$), of DLS. It is needless to mention that the errors come from the uncertainty of $P(qR)$, smearing, interference of the form factors between the like and unlike components, etc.

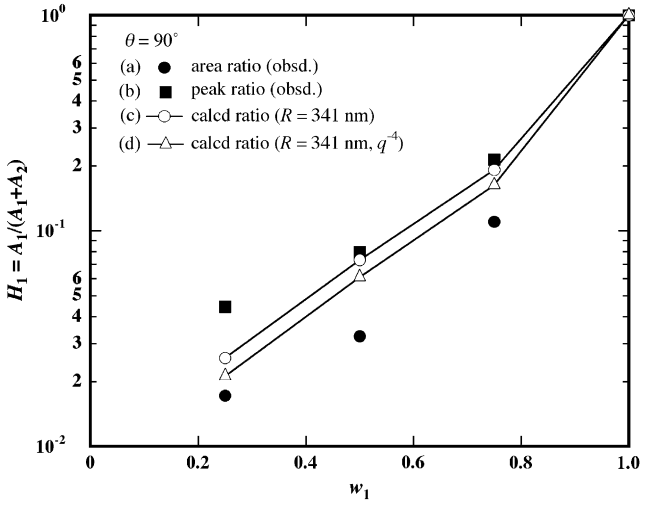

Fig. 10. The peak height fraction of L0, H_1, as a function of the weight fraction, w_1. (a) The observed area, (b) height, (c) calculated with the form factor of spheres, and (d) calculated with the asymptotic function. The lines are drawn for the eye.

4.3. Bimodal polymer solutions

A similar discussion to the case of latex solutions can be made for dilute polymer solutions. In this case, the form factor is, in principle, written by the so-called Debye function [23]

$$P_{\mathrm{D}}\left(qR_{\mathrm{g}}\right) = \frac{2}{u^2}\left[\mathrm{e}^{-u} - 1 + u\right], \quad u \equiv R_{\mathrm{g}}^2 q^2 \tag{35}$$

where R_{g} is the radius of gyration of the polymer chain. The first-order correlation function is given by

$$\begin{aligned} C^{(1)}(\tau, q) &\equiv \langle E(t,q)E^*(t+\tau,q)\rangle \\ &= cM_{\mathrm{w}}P_{\mathrm{D}}\left(qR_{\mathrm{g}}\right)\sum_{i,j}^{N}\exp\left[\mathrm{i}\mathbf{q}\cdot\delta\mathbf{r}_{ij}(t)\right] \\ &= cM_{\mathrm{w}}P_{\mathrm{D}}\left(qR_{\mathrm{g}}\right)\exp\left[-Dq^2\tau\right] \end{aligned} \tag{36}$$

Note that the scattering intensity is now proportional to the weight-average molecular weight of the polymer, M_{w}, and the mass concentration of the polymer, c. Hence, the amplitude is rewritten to

$$A_i(q) = c_i M_{\mathrm{w},i} P_{\mathrm{D}}\left(qR_{\mathrm{g},i}\right) = c_i R_{\mathrm{g},i}^2 P_{\mathrm{D}}\left(qR_{\mathrm{g},i}\right) \quad (\text{for a } \Theta\text{-solvent}) \tag{37}$$

This is in the case of a Θ-solvent. On the other hand, if the polymer chains are in a good solvent, $A_i(q)$ is given by

$$\begin{aligned} A_i(q) &= c_i M_{\mathrm{w},i} P_{\mathrm{F}}\left(qR_{\mathrm{g},i}\right) \\ &= c_i R_{\mathrm{g},i}^{5/3} P_{\mathrm{F}}\left(qR_{\mathrm{g},i}\right) \quad (\text{for a good solvent}) \end{aligned} \tag{38}$$

Here, because of the prediction of $R_{\mathrm{g}} \sim M_{\mathrm{w}}^{3/5}$ by Flory [24], we call $P_{\mathrm{F}}(qR_i)$ the Flory's asymptotic scattering function for a single polymer chain in a good solvent given by

$$P_{\mathrm{F}}\left(qR_{\mathrm{g}}\right) = \begin{cases} 1 & qR_{\mathrm{g}} \le \sqrt{3} \\ \dfrac{\left(\sqrt{3}\right)^{5/3}}{2}\left(qR_{\mathrm{g}}\right)^{-5/3} & qR_{\mathrm{g}} > \sqrt{3} \end{cases} \tag{39}$$

The cross-over $\sqrt{3}$ is obtained at the marginal point of $P_{\mathrm{D}}\left(qR_{\mathrm{g}}\right) = P_{\mathrm{F}}\left(qR_{\mathrm{g}}\right)$ at $q = 1/\xi = \sqrt{3}/R_{\mathrm{g}}$, where ξ is the correlation length. If the system consists of two-kinds of polymer

chains having different molecular weights, $M_{w,1}$ and $M_{w,2}$, the weight fractions of polymers 1 and 2 can be, in principle, evaluated from $G(\Gamma_i^{-1})$ with the same method discussed above by using Eqs. (37) and (38) in place of Eq. (21).

$$w_i = \frac{G(\Gamma_i)/R_{g,i}^2 P_D(qR_i)}{\sum_j G(\Gamma_j)/R_{g,j}^2 P_D(qR_j)} \tag{40}$$

for Θ-solvents, and

$$w_i = \frac{G(\Gamma_i)/R_{g,i}^{5/3} P_F(qR_i)}{\sum_j G(\Gamma_j)/R_{g,j}^{5/3} P_F(qR_j)} \tag{41}$$

for good solvents.

Fig. 11 shows (a) $g^{(2)}(\tau)$ and (b) $G(\Gamma^{-1})$ for polymer solutions in which PSs with $M_1 = 11.5 \times 10^3$ and $M_2 = 108.7 \times 10^3$ are mixed with different fractions. Here, not only the five fractions from 100/0 (P0) to 0/100 (P100), but also other mixtures with large portions of P0, i.e., 98/2, 96/4, and 90/10, were also investigated. As shown in the figure, the resolution of the distribution analysis does not seem to be good enough to separate the two modes originated from the P0 and P100, but DLS regards the system being a unimodal mixture with an average molecular weight, M_w. Fig. 12 shows the molecular weight dependence of the hydrodynamic radius, R_h. The exponent is 0.51, which is in good agreement with the prediction for a polymer solution in a Θ-solvent. This result suggests that the molecular weight ratio 108.7/11.5 ≈ 9.5 is not enough to apply this method. It should be noted here that the q-dependence of $A_i(q)$ is less significant in most of polymer solutions than in condensed particles. The calculated values of R_g's are 2.92 and 8.97 nm, respectively, for P0 and P100, for the Θ-condition. Here, the segment length of PS was chosen to be 0.68 nm [25]. The value of q at $\theta = 90°$ for cyclohexane at 34.5 °C is 0.020 nm^{-1}, indicating that the value of qR_g is much less or close to the criterion. Therefore, the contribution of the particle factor to the amplitude of the distribution function can be ignored and is simply dependent on the size of the polymer chains, i.e.,

$$A_i(q) = c_i R_{g,i}^2 P_D(qR_{g,i}) \approx c_i R_{g,i}^2 \quad \text{(for a } \Theta\text{-solvent)} \tag{42}$$

$$A_i(q) = c_i R_{g,i}^{5/3} P_F(qR_{g,i}) = c_i R_{g,i}^{5/3} \quad \text{(for a good solvent)} \tag{43}$$

This means that the peak height of $G(\Gamma_i^{-1})$ is weighted either R_g^2 or $R_g^{5/3}$, depending on the nature of solvent. It should be also noted that Eqs. (42) and (43) can be rewritten as

$$A_i(q) \approx c_i R_{g,i}^2 \propto c_i M_{w,i} \quad \text{(for a } \Theta\text{-solvent)} \tag{44}$$

$$A_i(q) \approx c_i R_{g,i}^{5/3} \propto c_i M_{w,i} \quad \text{(for a good solvent)} \tag{45}$$

Hence, it is concluded that $A_i(q)$ is dependent on the concentration and the molecular weight of the kind i, irrespective of the nature of the solvent. This result agrees with the treatment by Wu et al. [17]. However, if the product of R_g of the

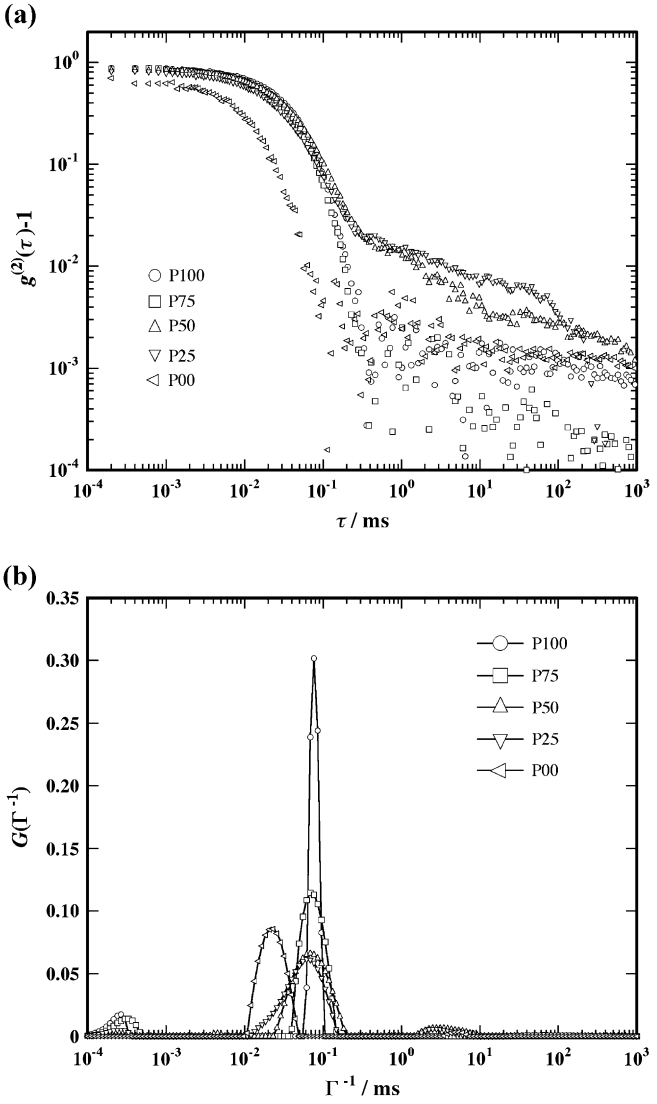

Fig. 11. Observed (a) correlation functions and (b) distribution functions for PS solutions having different compositions.

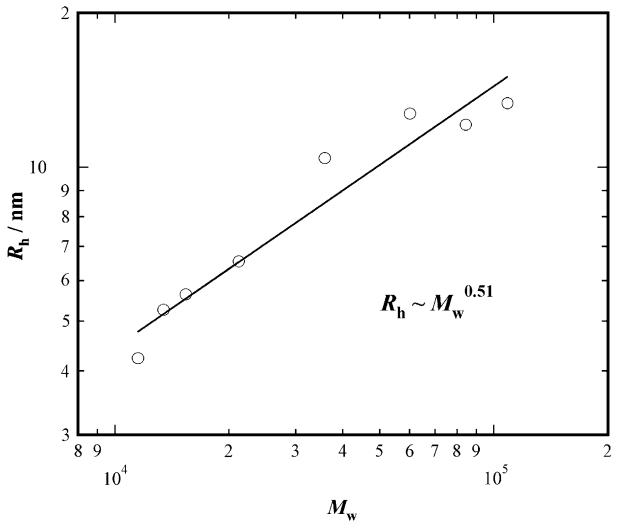

Fig. 12. Molecular weight dependence of the hydrodynamic radius, R_h.

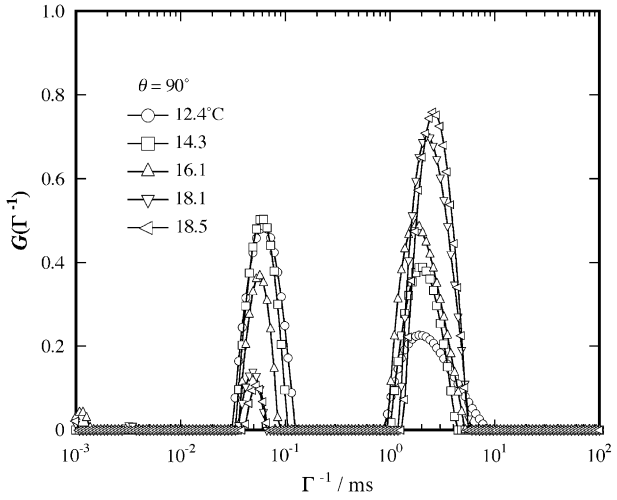

Fig. 13. The decay time distribution functions of 1.0 wt% poly(2-ethoxyethyl vinyl ether) (EOVE) aqueous solution at various temperatures.

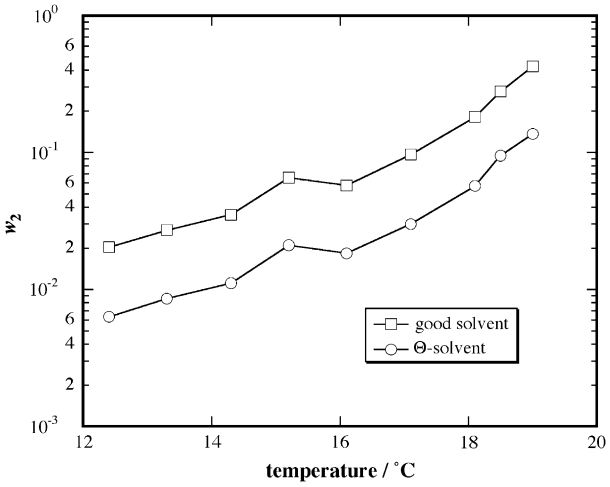

Fig. 14. Temperature variation of the fraction of the aggregate component, w_2, for 1.0 wt% poly(2-ethoxyethyl vinyl ether) (EOVE) aqueous solution.

sample and q of the DLS experiment is larger than the criterion, $qR_g \approx \sqrt{3}$, then the contribution of the form factor should be taken into account.

4.4. A polymer solution with aggregation

Polymers in a solution sometimes accompany their associated objects due to insufficient solvation. Okabe et al. observed a slow-mode component in an 1.0 wt% aqueous solution of poly(2-ethoxyethyl vinyl ether) (EOVE) [18]. The method discussed in this paper allows to evaluate the concentration (or the weight fraction) of this coagulants. Fig. 13 shows the $G(\Gamma^{-1})$s of 1.0 wt% EOVE solution at different temperatures. As shown in this figure, the fast component is dominant at 12 °C, while the slow component at $\Gamma^{-1} \approx 3$ ms becomes progressively dominant as temperature increases.

Fig. 14 shows the weight fraction of the slow component, w_2, i.e., the aggregated component, as a function of temperature. Here, the evaluation was made by two extreme cases, i.e., a Θ-condition (open circles) and a good-solvent condition (open squares). The values of w_2 increase from 0.0063 to 0.14 and from 0.020 to 0.43 of the solute, respectively, for the cases of a Θ-condition and a good-solvent condition. Note that the window of the w_2-value is of the factor of three, irrespective of temperature. This means that the fraction of large aggregates can be semi-quantitatively observed by this method.

5. Conclusion

A method to evaluate the weight fractions of the solute or dispersed species in a solution from the size distribution function $G(\Gamma)$ of DLS is proposed for the case of hard sphere mixtures as well as polymer mixtures having bimodal (or multi-modal) size distributions. It is found that the size distribution, $G(\Gamma)$, for spherical particles can be reconstructed by the position, Γ_i, and the amplitude, $A_i(q)$, with the following relationship:

$$G(\Gamma) = \sum_i \frac{A_i(q)}{\sum_j A_j(q)} \delta\left(\Gamma - D_i q^2\right) \tag{46}$$

$$w_i \propto \frac{G(\Gamma_i)}{R_i^3 \Phi^2(qR_i)} \tag{47}$$

where $A_i(q)$ is dependent on the system. The weight fractions, w_i, are then obtained by

$$w_1 = \frac{G(\Gamma_1)/R_1^3 \overline{\Phi}^2(qR_1)}{\sum_j G(\Gamma_j)/R_j^3 \overline{\Phi}^2(qR_j)} = \begin{cases} \dfrac{G(\Gamma_1)/R_1^3}{G(\Gamma_1)/R_1^3 + G(\Gamma_2)/R_2^3} & (qR_1, qR_2 \le 1.78) \\ \dfrac{G(\Gamma_1)/R_1^3\,[\mathrm{nm}^3]}{G(\Gamma_1)/R_1^3[\mathrm{nm}^3] + G(\Gamma_2)R_2\,[\mathrm{nm}]\,q^4\,[\mathrm{nm}^{-4}]/1.78^4} & (qR_1 < 1.78 \le qR_2) \\ \dfrac{G(\Gamma_1)R_1}{G(\Gamma_1)R_1 + G(\Gamma_2)R_2} & (1.78 \le qR_1, qR_2) \end{cases} \tag{48}$$

Eq. (48) indicates that the weight fraction of the components can be evaluated with the peak height (or area) and the peak position of the distribution function.

Similar to the case of dispersed particles in a dispersant, the concentration of polymers in a dilute solution can be evaluated with the following equations:

$$w_i \propto \frac{G(\Gamma_i)}{R_{g,i}^{\alpha_X} P_X(qR_i)} \tag{49}$$

where the subscript X stands for D (the Debye function, $P_D(qR_g)$ for a Θ-solvent) and for F (the Flory's asymptotic scattering function, $P_F(qR_g)$ for a good solvent). The exponent α_X also means $\alpha_X = 2$ (for a Θ-solvent) and $\alpha_X = 5/3$ (for a good solvent). Accordingly, $G(\Gamma)$ can be reconstructed with

$$A_i(q) = w_i M_i P_X\left(qR_{g,i}\right) = w_i R_{g,i}^{\alpha_X} P_X\left(qR_{g,i}\right) \tag{50}$$

with the observable quantity, R_g, and the evaluated value w_i.

This method was applied to characterize the fraction of aggregated component in a thermosensitive poly(2-ethoxyethyl vinyl ether) (EOVE) in aqueous solution. It was found that the fraction of the aggregates increased up to about 14% by increasing temperature.

References

[1] Berne BJ, Pecora R. Dynamic light scattering. N.Y.: Wiley; 1976.
[2] Chu B. Laser light scattering. Academic Press; 1991.
[3] Schmitz KS. An introduction to dynamic light scattering by macromolecules. New York: Academic Press; 1990.
[4] Pusey PN, van Megen W. Dynamic light scattering by non-ergodic media. Physica A 1989;157:705.
[5] Brown W. Dynamic light scattering, the methods and applications. Oxford: Clarendon Press; 1993.
[6] Shibayama M, Norisuye T. Gel formation analyses by dynamic light scattering. Bull Chem Soc Jpn 2002;75:641–59.
[7] Stepanek P. Data analysis in dynamic light scattering. In: Brown W, editor. Oxford: Oxford University Press; 1993 [chapter 4].
[8] Cohen RJ, Benedek GB. Immunoassay by light scattering spectroscopy. Immunochemistry 1975;12:963.
[9] Provencher SW, Stepanek P. Global analysis of dynamic light scattering autocorrelation functions. Part Part Syst Charact 1996;13:291.
[10] Gugliotta LM, Vega JR, Meira GR. Latex particle size distribution by dynamic light scattering: computer evaluation of two alternative calculation paths. J Colloid Interface Sci 2000;228:14–7.
[11] Vega JR, Gugliotta LM, Gonzalez VDG, Meira GR. Latex particle size distribution by dynamic light scattering: novel data processing for multiangle measurements. J Colloid Interface Sci 2003;261:74–81.
[12] Antony T, Saxena A, Roy KB, Bohidar HB. Laser light scattering immunoassay: an improved data analysis by CONTIN method. J Biochem Biophys Methods 1998;36:75–85.
[13] Kanao M, Matsuda Y, Sato T. Characterization of polymer solutions containing a small amount of aggregates by static and dynamic light scattering. Macromolecules 2003;36(6):2093.
[14] Wu C. Light scattering. In: Tanaka T, editor. New York: Academic Press; 2000. p. 1–56.
[15] Wu C, Bo S, Siddiq M, Yang G, Chen T. Laser light-scattering study of novel thermoplastics. 1. Phenolphthalein poly(aryl ether ketone). Macromolecules 1996;29:2989–93.
[16] Wu C, Siddiq M, Bo S, Chen T. Laser light-scattering study of novel thermoplastics. 2. Phenolphthalein poly(ether sulfone) (PES-C). Macromolecules 1996;29:3157–60.
[17] Wu C, Siddiq M, Woo KF. Laser light-scattering characterization of a polymer mixture made of individual linear chains and clusters. Macromolecules 1995;28:4914–9.
[18] Okabe S, Sugihara S, Aoshima S, Shibayama M. Heat-induced self-assembling of thermosensitive block copolymer. 2. Rheology and dynamic light scattering study. Macromolecules 2003;36:4099–106.
[19] Siegert AFJ. MIT Radiation Laboratory Report; 1943. No 465.
[20] Provencher SW. A constrained regularization method for investing data representated by linear algebraic or integral equations. Comput Phys Commun 1982;27:213–27.
[21] Porod G. Kolloid-Z 1951;124:83.
[22] Porod G. Kolloid-Z 1952;125:51.
[23] Debye P. J Phys Colloid Chem 1947;51:18.
[24] Flory PJ. Principles of polymer chemistry. Ithaca: Cornell Univ; 1953.
[25] Brandrup J, Immergut EH, Grulke EA. Polymer handbook. New York: Wiley; 1999.